# Journal of Materials Chemistry A

Accepted Manuscript


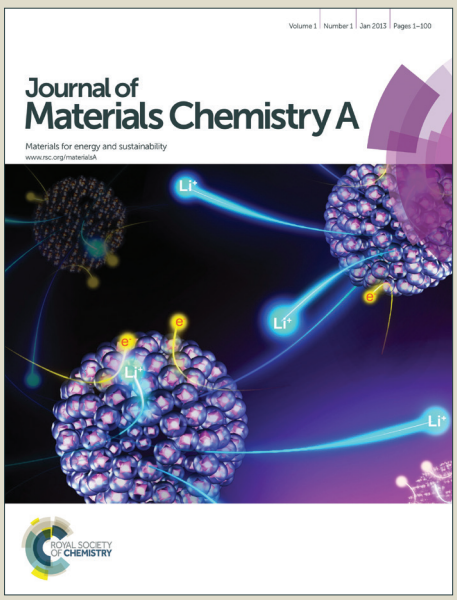





ROYAL SOCIETY OF CHEMISTRY

www.rsc.org/materialsA

# A Low Dimensional Composite of Hexagonal Lithium Manganese Borate ($LiMnBO_3$), a Cathode Material for Li-ion Batteries

By *Semih Afyon[a], Dipan Kundu[b], Azad J. Darbandi[c,d], Horst Hahn[c,d], Frank Krumeich[a], Reinhard Nesper[a]*

Dedicated to Professor Martin Jansen on the Occasion of his 70th Birthday.

[a] ETH Zurich, Department of Chemistry and Applied Biosciences,
CH-8093 Zurich, Switzerland

[b] University of Waterloo, Department of Chemistry,Waterloo, Canada

[c] KIT-TUD-Joint Research Laboratory Nanomaterials/Technische Universität Darmstadt, Germany

[d] Institute of Nanotechnology (INT), Karlsruhe Institute of Technology (KIT), Karlsruhe, Germany

E-mail: afyon@inorg.chem.ethz.ch
dkundu@waterloo.ca
krumeich@inorg.chem.ethz.ch
reinhard.nesper@inorg.chem.ethz.ch
azad.darbandi@web.de
horst.hahn@kit.edu

**[a]Address:** ETH Zurich, Laboratory of Inorganic Chemistry, Wolfgang Pauli Strasse 10, 8093Zurich Switzerland.

**Phone:** +41 446334623

**Fax:** +41 44 632 1149

Keywords: nanomaterial, borates, spray pyrolysis, Li-ion batteries

**Abstract**

The ultrasonic nebulized spray pyrolysis technique has been applied to synthesize amorphous nano-spheres that are further transformed into nano h-$LiMnBO_3$ with an average crystallite size of ~ 14 nm. A composite electrode of nano h-$LiMnBO_3$ with reduced graphite oxide and amorphous carbon delivers a high first discharge capacity of 140 mAh/g at C/15 rate within 4.5 – 2.0 V and retaining a discharge capacity of 110 mAh/g at the $25^{th}$ cycle. The dissolution of Mn into the electrolyte and the instability of highly delithiated phases during cycling are suggested as reasons limiting the cycling stability for h-$LiMnBO_3$. An improved cycling stability at higher capacities is expected via the combination of the particle size reduction, conductive network formation and the metal site doping strategies.

.

## 1. Introduction

Li-ion batteries lead in the portable electronics market by having the advantages of high voltage, high capacity, long cycle life and variable charge-discharge rates compared to the other battery technologies. However, the current cathode materials are still far away from satisfying the large energy density required for application in electric vehicles. An increase of specific energies may be achieved through novel high capacity cathode materials operating at high output voltages. Currently, $LiFePO_4$ could arguably be claimed as the most popular cathode material, but still quite limited with a theoretical specific capacity of 170 mAh/g[1, 2]. However, this compound exemplifies both, how transition metal ions can be bound efficiently into stable networks by linking through phosphate groups and how compounds of low electronic conductivity may be utilized successfully. Borate groups fulfill a similar function to phosphate but they have lower specific weight resulting in higher capacities. For instance, $LiMnBO_3$ has a theoretical capacity of ~ 222 mAh/g for the $Mn^{2+}/Mn^{3+}$ redox couple, whereas the phosphate counterpart, $LiMnPO_4$, is limited to ~ 171 mAh/g.

The first investigation of the use of transition metal borates, $LiMBO_3$ (M=Fe, Mn, Co) as cathode materials for Li-ion batteries was done by Legagneur et al., and particularly, for the hexagonal phase of $LiMnBO_3$, 0.02 lithium per formula unit were extracted at the first charge cycle in their study[3]. The electrochemical activity for the monoclinic phase of $LiMnBO_3$ was first demonstrated by Kim et al.; where the carbon composite electrode material synthesized by a conventional solid state method delivered a second discharge capacity of 100 mAh/g at C/20[4]. There are also more recent reports, with success to some extent, on the utilization of the monoclinic phase and mixed phases as cathode materials[5-8]. Some other investigations on various borate based electrode materials can also be found in literature[9-12].

Most research on the hexagonal-$LiMnBO_3$ alone showed low charge/discharge capacities within quite large potential windows[3, 13-18]. Chen et al. demonstrated a charge/discharge capacity of only 75.5 mAh/g for h-$LiMnBO_3$ with a huge polarization at ~ C/40 rate in a potential window of 4.8 – 1.0 V[18]. In another report, Li et al. reported a first discharge capacity of 90.7 mAh/g for carbon coated h-$LiMnBO_3$ within 4.8 – 1.25 V at a rate of C/20[7]. However, irreversible capacity losses in the first cycle, probably stemming from the decomposition of the electrolyte, could be observed in those studies[7, 17, 18], and the source of the delivered capacities might be conversion reactions or pseudo-capacitance rather than the lithiation/delithiation of h-$LiMnBO_3$ in the large designated potential ranges used.

Low ionic and electronic conductivities of borates are considered as reasons for their poor electrochemical performance as energy storage materials. There is good reason that this should be circumvented through the employment of nano-particles and conductive coatings. In addition, the utilization of nanoparticles in electrodes decreases the diffusion paths for $Li^+$ ions and enhances electron hopping, and thus, considerably improves charge/discharge capacities and cycling stability of the otherwise poorly conducting and performing materials. By doing so, we previously demonstrated a high capacity of 145 mAh/g within 4.7–1.7 V for nano-particles of h-$LiMnBO_3$ coated reduced graphite oxide (RGO) coated [19]. Here, we take the electrochemical performance of h-$LiMnBO_3$ a step further and present a novel carbon/nano-composite of h-$LiMnBO_3$ giving a higher capacity in a narrower potential window. The material obtained by spray pyrolysis consists of nano-spheres and was further treated with reduced graphite oxide to obtain a corresponding composite electrode. The carbon / h-$LiMnBO_3$ nano-composite delivers a first discharge capacity of 140 mAh/g at C/15 rate within 4.5 – 2.0 V and largely maintains this

capacity within the first 50 cycles. These are the most advanced results obtained so far for h-$LiMnBO_3$ to the best of our knowledge.

## 2. Experimental Section

*2.1 Synthesis*:

Ultrasonic nebulized spray pyrolysis technique is applied for the synthesis of amorphous nano-spheres. The chemicals used for preparing the precursor solution are $LiOH.H_2O$ (99.99%, Sigma-Aldrich), $H_3BO_3$ (99.97%, Sigma-Aldrich), and $Mn(CH_3COO)_2.(H_2O)_4$ (99.99%, Sigma-Aldrich) in stoichiometric amounts. $LiOH.H_2O$ and $H_3BO_3$ were dissolved in deionized water at 40°C and the pH-value of the solution was adjusted subsequently to 6 by adding formic acid. Separately, $Mn(CH_3COO)_2.(H_2O)_4$ was dissolved in deionized water at 25 °C. These two solutions were mixed together and a transparent precursor is consequently achieved. The apparatus used for the spray pyrolysis consists of an atomization chamber, a pyrolysis zone, and a chamber for powder collection. The precursor solution was in contact with a $(Pb(Zr,Ti)O_3)$ transducer at a frequency of 1.7 MHz for the ultrasonic nebulization. The nebulized precursor droplets were continuously delivered to the pyrolysis zone by a total gas flow rate of 5 l/min. The carrier gas consisted of 80% Ar and 20% $H_2$, in order to avoid the oxidation of $Mn^{2+}$ to $Mn^{3+}$. The pyrolysis zone consists of an alumina tube placed into a resistively heated furnace. A paper filter was used to collect the particles. The temperature of the filter was held above 100 °C in order to suppress water condensation. A vacuum pump and an automatically operated reducing valve were used to maintain total pressure within the system at 0.75 atm. The powder was synthesized at temperatures of 650 °C.

For the preparation of the composite electrode material, ~ 70 wt-% amorphous nano-spheres obtained by the spray pyrolysis technique, ~ 19 wt-% graphite oxide and ~ 11 wt-% lactose had been mixed and ball-milled in acetone that was followed by heat treatments at 400 °C

(6 hrs) and 500 °C (2 hrs) with a heating rate of 25 °C /h under Argon. Combustion-infrared spectroscopy analysis (LECO instruments, ETH LOC Micro-Laboratory) revealed a final carbon content of ~ 21.5 wt-% for the composite material.

*2.2 Characterization*:

STOE Stadi P diffractometer equipped with a germanium monochromator and $CuK_{\alpha 1}$ radiation (operated at 35 mA, 35kV) was used to record Powder X-ray diffraction patterns of the samples. The Scherrer equation (crystallite size = 0.9 $\lambda$ / ($\beta$ cos $\theta$), where $\lambda$ is the wavelength of incident X-rays, $\beta$ is the full width at the half maximum of the (111) peak for h-$LiMnBO_3$, and $\theta$ is the Bragg angle) was used to estimate the average crystallite sizes of h-$LiMnBO_3$ in the composite material.

Scanning electron microscopy (SEM) analysis of samples were performed with a Zeiss Gemini 1530 operated at 1 kV. (Scanning) transmission electron microscopy ((S) TEM) analysis were carried out with a CM30ST (FEI; $LaB_6$ cathode) and a Tecnai F30 microscope (FEI; field emission gun), both operated at 300 kV, point resolution of ~ 2Å. The F30 microscope is equipped with an energy-dispersive X-ray spectrometer (EDXS; EDAX) and an electron energy-loss spectrometer (EELS; Gatan).

2.3 *Electrochemical tests*:

(80 wt-%) composite material, (10 wt-%) conductive carbon (Super P® Li Timcal) and 10 wt-% PVDF binder were mixed, and a slurry in N-Methyl-2-pyrrolidone (NMP) was prepared by ultrasonic dispersion. The slurry was cast on Ti current collectors that were dried at 100 $^{o}$C under vacuum afterwards. The final electrodes approximately contained 3-4 mg active material (a loading of ~ 4 mg/cm$^2$). Li metal disks that were cut from a 0.75 mm-thick ribbon (Aldrich) served as anodes , and 1M solution of $Li[(C_2F_5)_3PF_3]$ in EC:DMC (1:1) (Merck, LF-30

SelectiLyte™) was as the electrolyte. Any major capacity contribution from the oxidation of the electrolyte is not expected due to its reported stability within the potential window of our interest[20]. Swagelok type of cells, constructed in an Ar filled glove-box, were used for the electrochemical tests. The cells were cycled within 4.5 – 2.0 V in a galvanostatic protocol at rates of C/20 and C/15. Rate capability tests were performed in ~ 5 cycle blocks at varying rates C/20, C/10, C/5, C/3, and again back to C/20; the rates were consecutively changed after a discharging section.

**3. Results and Discussion**

The product obtained by the ultrasonic nebulized spray pyrolysis technique consists of amorphous nano-spheres as evidenced by X-Ray powder diffraction and electron microscopy analysis (**Fig. 1, 2, 3 and 4**). A high background lacking any strong reflections is found in the XRD powder pattern of the sample, indicating the amorphous nature (**Fig. 1a-green**). After the heat treatment applied to form the composite material, the hexagonal phase of $LiMnBO_3$ was obtained. The broadened diffraction peaks hint the presence of h-$LiMnBO_3$ nano-particles in the composite material. All diffraction peaks in the XRD pattern of the composite material can be matched the theoretical pattern of h-$LiMnBO_3$ (ICSD 94318), and no residual diffraction peaks indicating any impurities could be observed (**Fig. 1a**). The electron diffraction pattern (**Fig. 2a**) of the composite material further confirms the presence of nano h-$LiMnBO_3$, as the d-values from the pattern matching to the theoretical plane distances of hexagonal $LiMnBO_3$. The hexagonal phase (space group: P-6, $a$ = 8.172(1) Å, $c$ = 3.1473(6) Å, $V$ = 182.02(5) $Å^3$)[3] (**Fig. 1b**) contains $MnO_5$ square pyramids that are connected to each other by sharing the equatorial edges of the pyramids. Planar $BO_3$ units link these chains of $MnO_5$ polyhedra running along the

c-axis together with the parallel strands of $LiO_4$ tetrahedra. The preferred diffusion path for $Li^+$ ions is also along this axis according to the previous theoretical work by Kim et al.[4].

Scanning electron microscopy (SEM) images of the amorphous nano-spheres and carbon/nano h-$LiMnBO_3$ composite are displayed in **Fig. 3**. The sizes of the amorphous nano-spheres mostly appear to be in the range of 200-300 nm; however, spheres with larger diameters in sub-micron regime could also be found in the images (**Fig. 3a & 3b, S1**). The spherical morphology of the particles was lost after ball-milling and consecutive heat treatment, and a homogeneous composite with carbon was obtained (**Fig. 3c & 3d, S1**). The average particle size for h-$LiMnBO_3$ crystallites was reduced, as it can be deduced from SEM images. This finding is further confirmed by the broadening of (111) reflection and the average crystallite size is found to be ~ 14 nm that is the smallest reported so far for h-$LiMnBO_3$.

Transmission electron microscopy (TEM) images of the nano-spheres obtained by spray-pyrolysis prove the amorphous nature with a lack of any order even in the nanometer range which is consistent with the findings from the bulk characterization (**Fig. 4a & 4b**). Electron diffraction patterns without any diffraction rings further support this point (**Fig. 2b**). The presence of manganese and boron in the nano-spheres is further confirmed by electron energy loss spectroscopy (EELS) (**Fig. S2**). TEM images of the carbon / nano h-$LiMnBO_3$ composite are displayed in **Figure 4c & 4d**. After the ball-milling and consecutive heat treatment, lattice fringes of the (111) planes of h-$LiMnBO_3$ are evident in high resolution TEM images (**Fig. 4d**). Stacking faults are present that indicate a certain amount of disorder in the crystallite. The size observed for the h-$LiMnBO_3$ nano-crystallites in TEM seems to be in range with the prediction from the broadening of (111) reflection, and some particle fragments that are even smaller than 5 nm are also visible in the high resolution TEM images. The coverage of nano h-$LiMnBO_3$ by

reduced graphite oxide (RGO) and amorphous carbon, as well as the network formation can be clearly identified. Such a network formation is expected to bring about enhanced local and long range conductivity and an increase of mechanical stability of the electrode. The interlayer distance found for the coating material on nano h-$LiMnBO_3$, ~ 3.6 Å**,** provides evidence for the presence of reduced graphite oxide (RGO) that is in direct contact with the particle surfaces.

The galvanostatic charge/discharge curves for the amorphous nano-spheres are displayed in in **Figure 5a**. The cell was cycled within 4.5 – 2.0 V at a rate of C/20. The working electrode consisted of 70 wt-% amorphous nano-spheres, 20 wt-% conductive carbon (Super P® Li Timcal) and 10 wt-% PVDF binder. The amorphous nano-spheres can be delithiated delivering a first charge capacity of ~ 61 mAh/g at an average voltage of 4.05 V; however, the lithiation/delithiation process is not reversible in the subsequent cycles and the capacity drastically fades at each cycle. The huge polarization is also very evident similar to the observations in previous investigations, where crystalline or micro-crystalline h-$LiMnBO_3$ was employed as a cathode material for Li-ion batteries. The cycling stability and the charge/discharge capacities are considerably improved for the carbon / nano h-$LiMnBO_3$ composite electrode. **Fig. 5b** depicts the first ten galvanostatic charge/discharge curves of the C/nano h-$LiMnBO_3$ composite that were obtained at C/15 rate in a potential window between 4.5 and 2.0 V. The working electrode contained approximately 80 wt-% composite material, 10 wt-% conductive carbon (Super P® Li Timcal) and 10 wt-% PVDF binder. The first discharge capacity is ~ 140 mAh/g and a fairly stable cycling is maintained with a discharge capacity of 110 mAh/g at the $25^{th}$ cycle. The average discharge capacity loss is only ~ 0.9 % per cycle for the first 50 cycles (**Fig. 5c**) . The dQ/dV plot for C/nano h-$LiMnBO_3$ composite shows broad oxidation and reduction peaks with apparent polarization (**Fig. 6**); yet, the degree of polarization

on lithiation/delithiation of $LiMnBO_3$ has been noticeably diminished in this study compared to the earlier investigations on this compound. The oxidation peak appears at ~ 3.8 V, whereas, the reduction peak is found at ~ 2.8 V, and both oxidation and reduction processes are spread to the whole voltage range.

The XRD powder pattern of a cycled electrode of the C/nano h-$LiMnBO_3$ composite is shown in **Figure 7**. As stated before, the composite electrode consisted of nano-crystalline h-$LiMnBO_3$ covered with amorphous carbon and RGO. Upon extended cycling, no obvious diffraction peaks could be found in the XRD powder pattern, which indicates the complete amorphization of $LiMnBO_3$. This point is further confirmed by electron microscopy analysis (**Fig. S4 & S5**). The amorphization of the active phase causes capacity fading as a result of the contact losses within the electrode, and this might also point to phase decomposition; though, the latter point is hard to be ultimately stated by diffraction studies due to the amorphous nature of the decomposition products.

Previously, Mn dissolution into the electrolyte upon cycling was suggested as one of the reasons for the unstable cycling of $LiMnBO_3$, and for the monoclinic phase, the charged state instability and Mn dissolution were experimentally demonstrated by other investigators[8]. For the hexagonal phase, similar problems seem to occur, as well. **Figure 8** shows the SEM-EDX analysis of the material deposited on the Li anode from a cell of C/nano h-$LiMnBO_3$ composite after 50 cycles. The manganese signal is found along with other elemental signals stemming from the electrolyte. The manganese dissolution into the electrolyte results in capacity fading at each cycle by a joint effect of the loss of active mass on the cathode and the deposition of an insulating layer on the anode. Furthermore, a discharge capacity (~ 201 mAh/g) close to the theoretical capacity was obtained with lower current rates (e.g. C/20) at rate capability tests, but,

tapping more capacity, reaching to highly delithiated phases in other words, undesirably deteriorates the cycling stability (**Fig. S3**). This finding further supports the possible instability of the highly charged states for h-$LiMnBO_3$ that is similar to the case in m-$LiMnBO_3$.

The enhanced properties reported here for h-$LiMnBO_3$ can be mainly attributed to further reduction of particle sizes compared to the earlier investigations and to the sophisticated conductive network formation. The utilization of nano h-$LiMnBO_3$ with an average particle size of ~ 14 nm in the electrode is expected to shorten the length of diffusion paths for $Li^+$ ions and augment electron-hopping. The conductive network formed by reduced graphite oxide (RGO) and amorphous carbon also facilities electron hopping and $Li^+$ ion transport. Thus, a high capacity in a narrower potential window and reduced kinetic polarization compared to the other studies were obtained. In addition, the RGO network could act as a protective barrier against the by-products that might form during cycling[21-24]. The mechanical stability gained via network formation is also helpful in terms of preserving the interconnectivity between the nano particles during cycling. Yet, cycling stability remains a problem for h-$LiMnBO_3$, despite the enhancement of performance presented here. Phase decomposition and Mn dissolution into the electrolyte during cycling, which is likely to occur due to the instability of highly delithiated phases[4, 8] and their reactions with electrolyte, might be suppressed via metal side doping. For the monoclinic phase (m-$LiMnBO_3$)[8] and for a number of cathodes[25-28], partial Mg substitution has been already demonstrated to effectively suppress the Mn dissolution and capacity fading by keeping the structural integrity. A similar strategy, together with the utilization of nano-particles and the improved protective coatings, might be expected to bring about a cycling stability that is good enough to enable practical implementations.

## 4. Conclusion

Amorphous nano-spheres synthesized by ultrasonic nebulized spray pyrolysis technique were used as precursors to obtain a novel carbon composite of h-$LiMnBO_3$. The composite material consisted of nano h-$LiMnBO_3$ with an average crystallite size of ~ 14 nm embedded in a conductive matrix of reduced graphite oxide (RGO) and amorphous carbon. The carbon / nano h-$LiMnBO_3$ composite delivered a discharge capacity of ~ 140 mAh/g at C/15 rate within 4.5 – 2.0 V and showed a fairly stable cycling with an average discharge capacity loss of ~ 0.9 % per cycle for the first 50 cycles. The degree of polarization was also diminished compared to the earlier reports. The improved electrochemical performance for h-$LiMnBO_3$ has been linked to the small particle size and to the close setting of small particles in the conductive network. The ex-situ investigations made on cycled electrode materials provided evidence for Mn dissolution into the electrolyte that might be related to the instability of highly delithiated phases. The rate capability measurements further strengthened this hypothesis. The metal site doping providing structural integrity at the charged states and the employment of sophisticated protective coatings limiting the reactions between the electrolyte and the delithiated phases are likely to provide a more stable cycling at higher charge/discharge capacities. Nevertheless, to the best of our knowledge, these are the most advanced results obtained for h-$LiMnBO_3$ until now, setting a reasonable example for the operation of $LiMnBO_3$ in a narrow potential window being encouraging for the possible practical applications.

## Figures

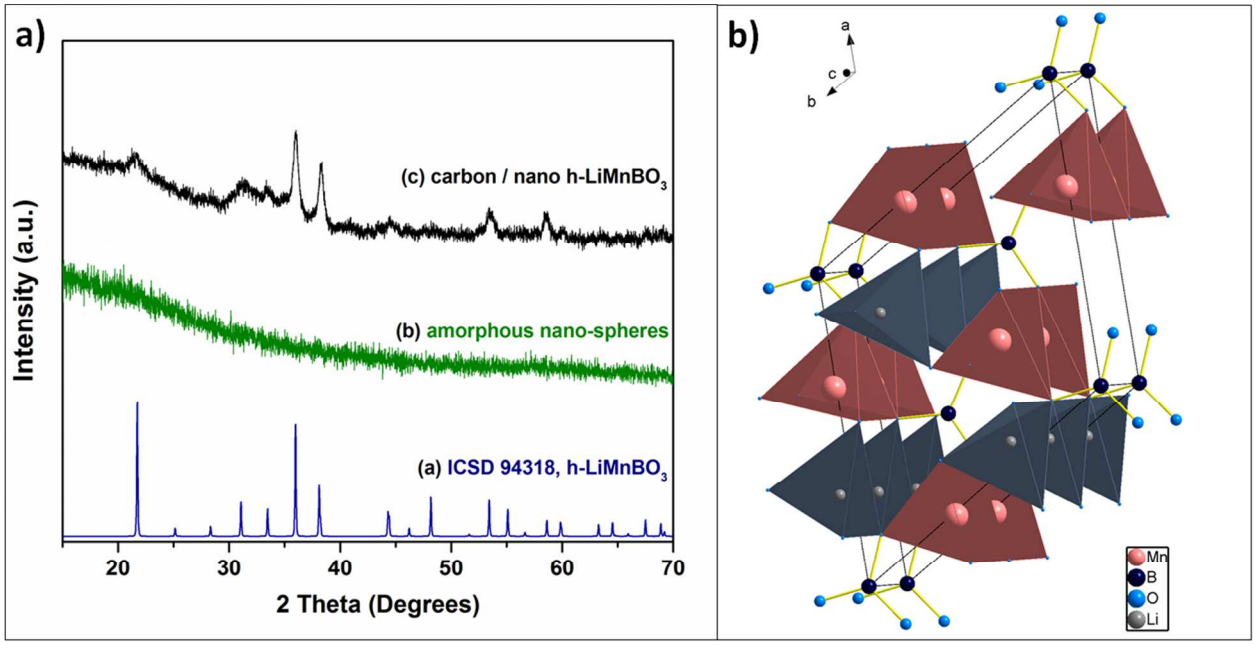


**Figure 1 a)** XRD powder patterns of h-$LiMnBO_3$: calculated (blue), spray-pyrolysis product (green), and carbon / nano h-$LiMnBO_3$ glass composite (black), **b)** View of the crystal structure of h-$LiMnBO_3$ along skew [001].

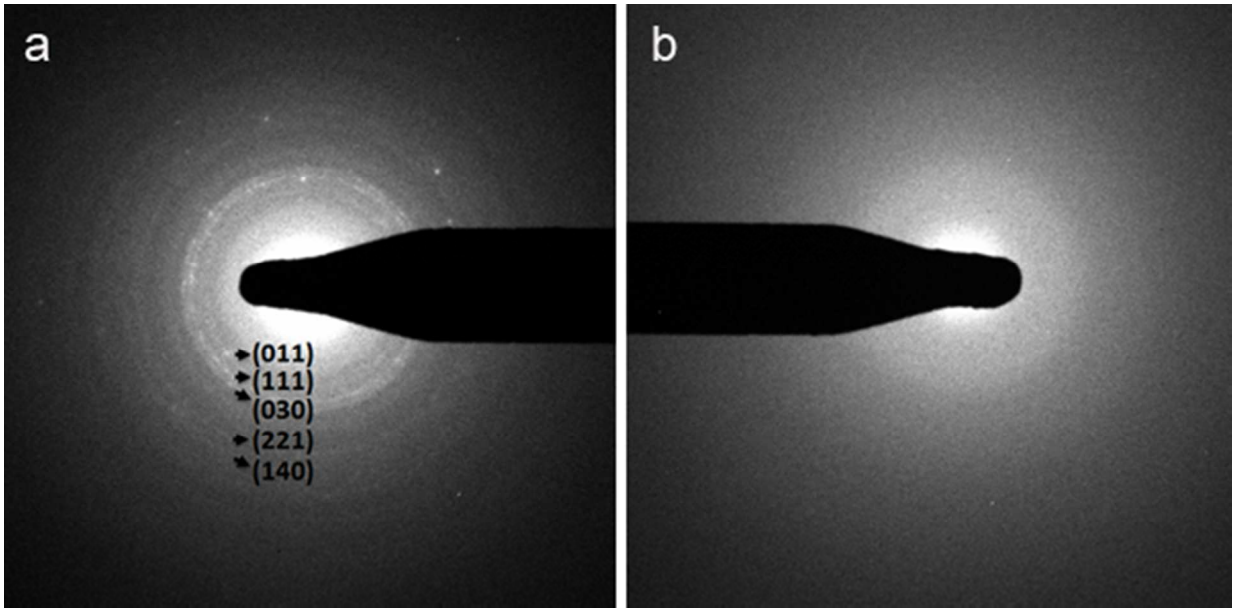


**Figure 2.** Electron diffraction patterns of a) carbon / nano h-$LiMnBO_3$ composite with identified diffraction rings and b) nano-spheres lacking diffraction rings showing their amorphous nature.

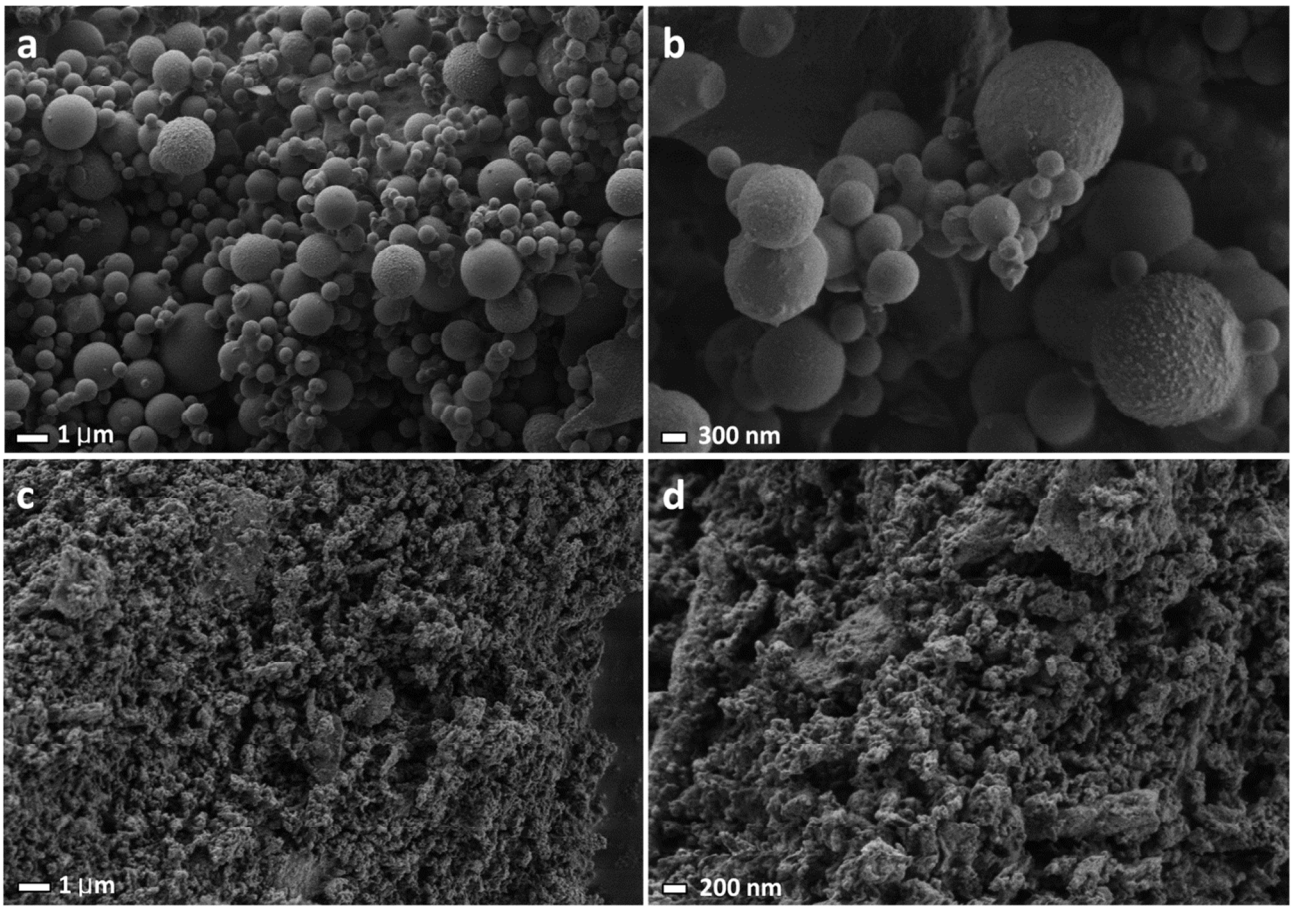


**Figure 3** Scanning electron microscopy (SEM) images of a) & b) amorphous nano-spheres, c) & d) carbon / nano h-$LiMnBO_3$ composite.

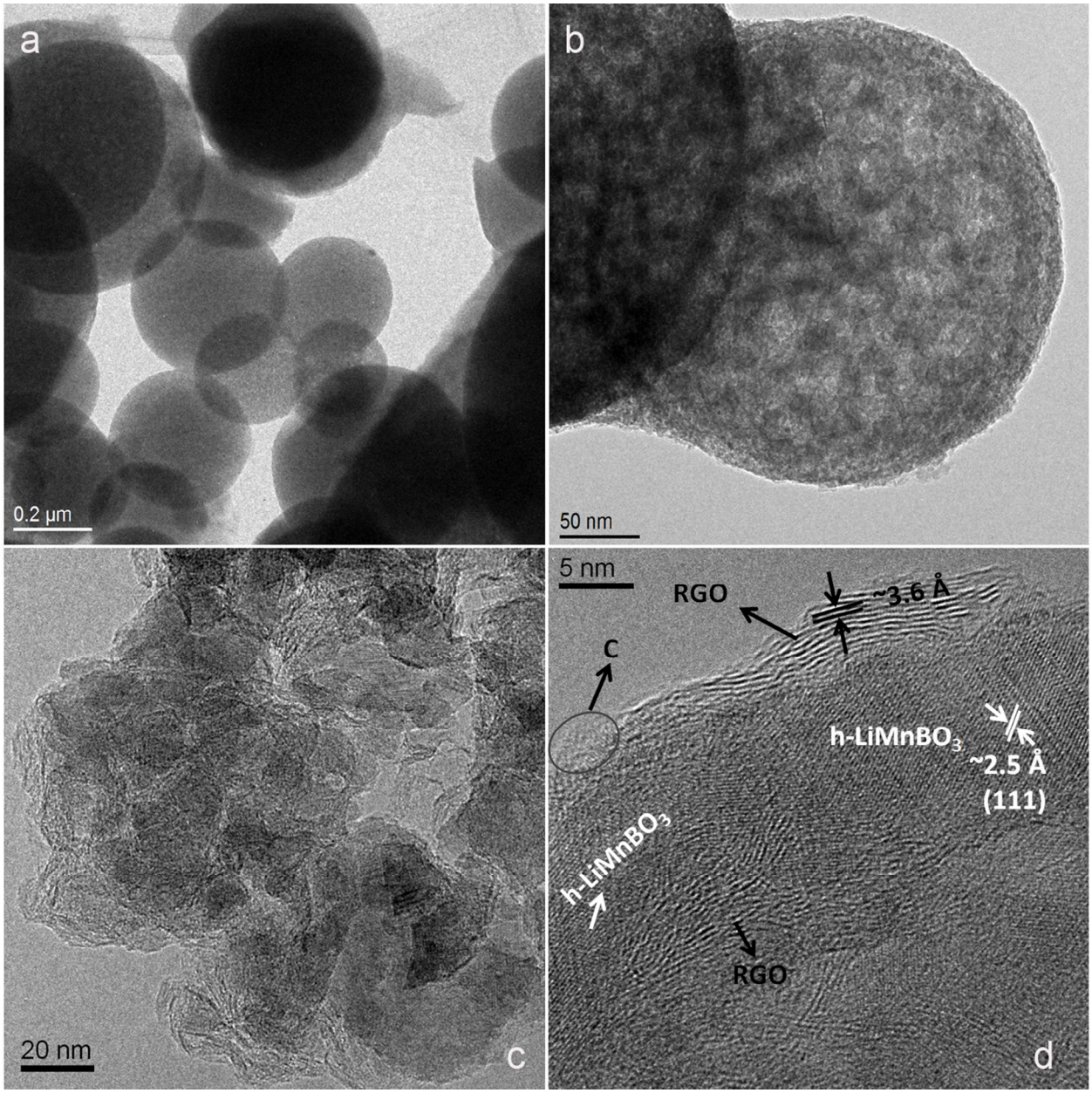


**Figure 4** Transmission electron microscopy images (TEM) displaying a) the morphology of particles obtained via spray-pyrolysis, b) the amorphous nature of nano-spheres, c) carbon / nano h-$LiMnBO_3$ composite material, d) a fine coating of reduced graphite oxide (RGO) and amorphous carbon on nano h-$LiMnBO_3$ particles.

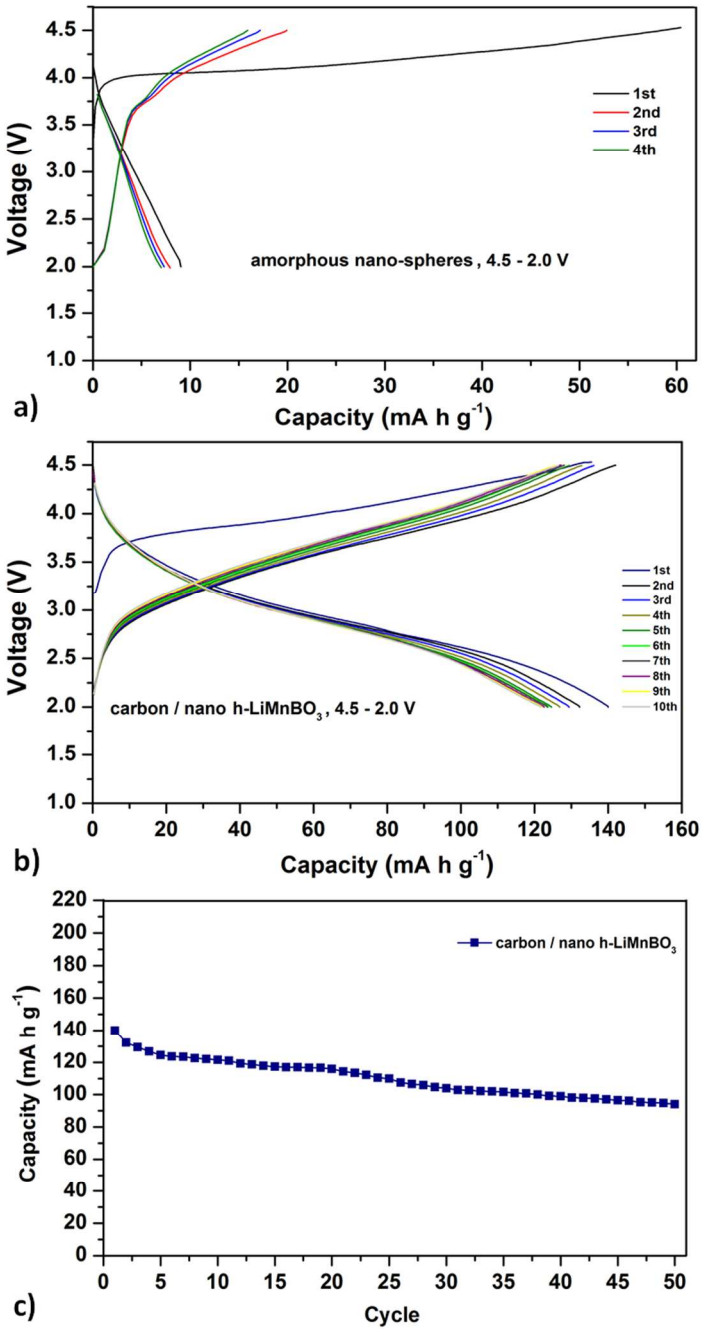


**Figure 5** a) The first four charge/discharge curves of amorphous nano-spheres in a potential window of 4.5 – 2.0 V at C/20 rate, b) the first ten charge/discharge curves of the carbon / nano h-$LiMnBO_3$ composite in a potential window of 4.5 – 2.0 V at C/15 rate, c) discharge capacity vs. cycle number for the carbon / nano h-$LiMnBO_3$ composite at a rate of C/15 rate within 4.5 – 2.0 V.

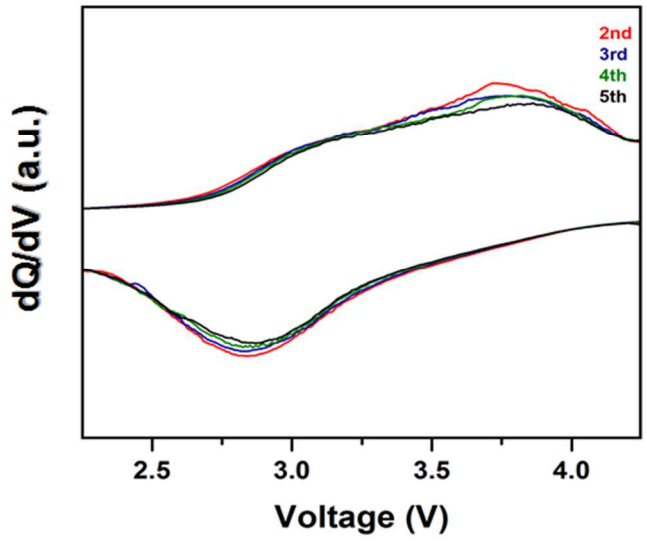


**Figure 6** The differential capacity plot for the galvanostatic cycling of the carbon / nano h-$LiMnBO_3$ composite.

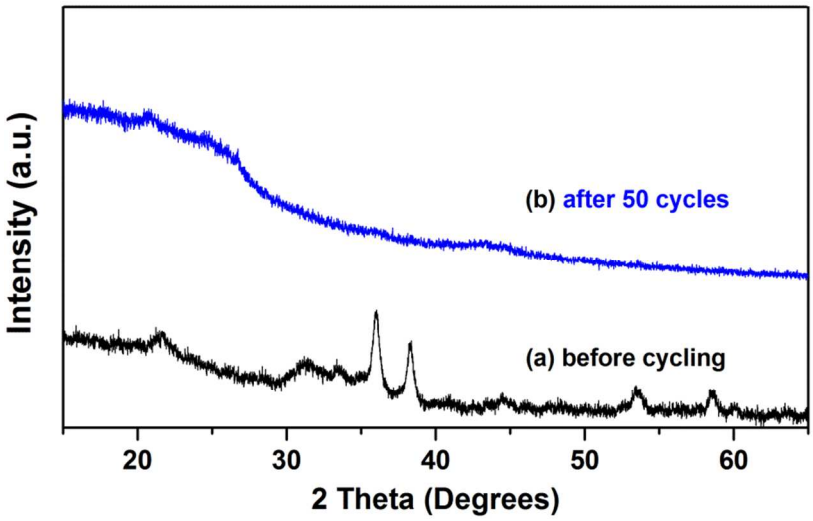


**Figure 7** XRD powder pattern of an electrode of the carbon / nano h-$LiMnBO_3$ composite in the discharged state after 50 cycles.

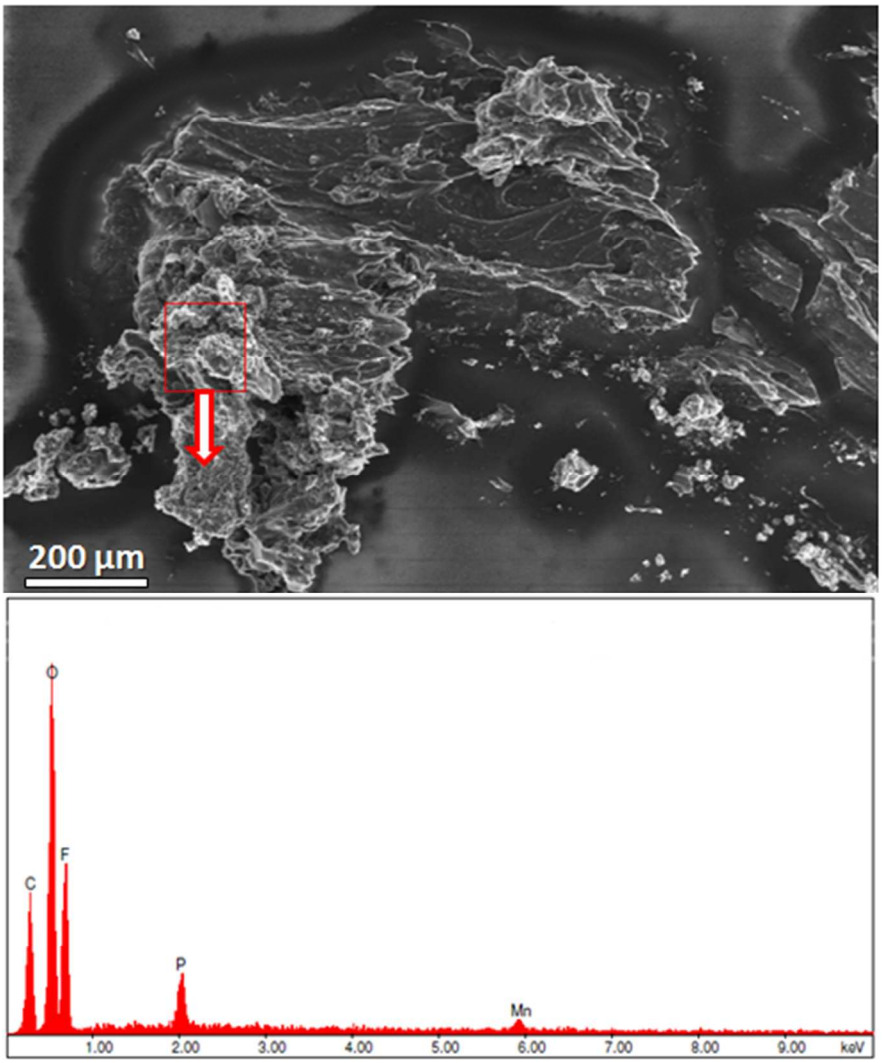


**Figure 8** Scanning electron microscopy (SEM) image of a deposit on Li anode, and energy dispersive X-ray (EDX) spectrum of the marked region confirming the manganese dissolution (the deposit taken from a cell of carbon / nano h-$LiMnBO_3$ composite after 50 cycles).

1. A. K. Padhi, K. S. Nanjundaswamy and J. B. Goodenough, *J Electrochem Soc*, 1997, **144**, 1188-1194.
2. H. Matsui, T. Nakamura, Y. Kobayashi, M. Tabuchi and Y. Yamada, *J Power Sources*, 2010, **195**, 6879-6883.
3. V. Legagneur, Y. An, A. Mosbah, R. Portal, A. L. La Salle, A. Verbaere, D. Guyomard and Y. Piffard, *Solid State Ionics*, 2001, **139**, 37-46.
4. J. C. Kim, C. J. Moore, B. Kang, G. Hautier, A. Jain and G. Ceder, *J Electrochem Soc*, 2011, **158**, A309-A315.
5. V. S. Stafeeva, R. V. Panin, M. V. Lobanov and E. V. Antipov, *Russ Chem B+*, 2013, **62**, 374-379.
6. K. J. Lee, L. S. Kang, S. Uhm, J. S. Yoon, D. W. Kim and H. S. Hong, *Curr Appl Phys*, 2013, **13**, 1440-1443.
7. S. L. Li, L. Q. Xu, G. D. Li, M. Wang and Y. J. Zhai, *J Power Sources*, 2013, **236**, 54-60.
8. J. C. Kim, X. Li, C. J. Moore, S.-H. Bo, P. G. Khalifah, C. P. Grey and G. Ceder, *Chem Mater*, 2014, **26**, 4200-4206.
9. A. I. Palos, M. Morcrette and P. Strobel, *J Solid State Electr*, 2002, **6**, 134-138.
10. S. Okada, T. Tonuma, Y. Uebo and J. Yamaki, *J Power Sources*, 2003, **119**, 621-625.
11. D. H. Seo, Y. U. Park, S. W. Kim, I. Park, R. A. Shakoor and K. Kang, *Phys Rev B*, 2011, **83**.
12. S. Afyon, M. Worle and R. Nesper, *Angew Chem Int Edit*, 2013, **52**, 12541-12544.
13. J. L. Allen, K. Xu, S. S. Zhang and T. R. Jow, *Materials for Energy Storage, Generation and Transport*, 2002, **730**, 9-14.
14. ARAVINDAN, #160, V., KARTHIKEYAN, K., AMARESH, S., LEE and Y. S., *LiMnBO[3]/C: A Potential Cathode Material for Lithium Batteries*, Korean Chemical Society, Seoul, COREE, REPUBLIQUE DE, 2010.
15. L. Chen, Y. Zhao, X. An, J. Liu, Y. Dong, Y. Chen and Q. Kuang, *J Alloy Compd*, 2010, **494**, 415-419.
16. R. Ma, L. Y. Shao, K. Q. Wu, M. M. Lao, M. Shui, C. Chen, D. J. Wang, N. B. Long, Y. L. Ren and J. Shu, *Ceram Int*, 2013, **39**, 9309-9317.
17. V. Aravindan, K. Karthikeyan, S. Amaresh and Y. S. Lee, *B Kor Chem Soc*, 2010, **31**, 1506-1508.
18. L. Chen, Y. M. Zhao, X. N. An, J. M. Liu, Y. Z. Dong, Y. H. Chen and Q. Kuang, *J Alloy Compd*, 2010, **494**, 415-419.
19. S. Afyon, D. Kundu, F. Krumeich and R. Nesper, *J Power Sources*, 2013, **224**, 145-151.
20. M. Schmidt, U. Heider, A. Kuehner, R. Oesten, M. Jungnitz, N. Ignat'ev and P. Sartori, *J Power Sources*, 2001, **97–98**, 557-560.
21. K. S. Lee, S. T. Myung, K. Amine, H. YashiroB and Y. K. Sun, *J Mater Chem*, 2009, **19**, 1995-2005.
22. B. J. Li, H. Q. Cao, J. Shao and M. Z. Qu, *Chem Commun*, 2011, **47**, 10374-10376.
23. S. Afyon, C. Mensing, F. Krumeich and R. Nesper, *Solid State Ionics*, 2014, **256**, 103-108.
24. C. Nithya and S. Gopukumar, *J Mater Chem A*, 2014, **2**, 10516-10525.
25. Q. Lu, G. S. Hutchings, Y. Zhou, H. L. L. Xin, H. M. Zheng and F. Jiao, *J Mater Chem A*, 2014, **2**, 6368-6373.
26. F. Nobili, F. Croce, R. Tossici, I. Meschini, P. Reale and R. Marassi, *J Power Sources*, 2012, **197**, 276-284.

27. R. Singhal, M. S. Tomar, J. G. Burgos and R. S. Katiyar, *Ieee Int Ferro*, 2008, 345-346.
28. D. Capsoni, M. Bini, G. Chiodelli, V. Massarotti, M. C. Mozzati and C. B. Azzoni, *Solid State Commun*, 2003, **125**, 179-183.

**Table of contents entry**

Nano h-$LiMnBO_3$ composite delivers a high first discharge capacity of 140 mAh/g at C/15 rate within a reduced potential window.